Journal of Hydrology 591 (2020) 125689

Contents lists available at ScienceDirect

Journal of Hydrology

journal homepage: www.elsevier.com/locate/jhydrol

Research papers

The relative contribution of vegetation greening to the hydrological cycle in the Three-North region of China: A modelling analysis

Shanshan Meng [a,b], Xianhong Xie [a,*], Bowen Zhu [a], Yibing Wang [a]

[a] State Key Laboratory of Remote Sensing Science, Faculty of Geographical Science, Beijing Normal University, Beijing 100875, China
[b] College of Geography and Environment, Shandong Normal University, Jinan 250014, China

ARTICLE INFO

Keywords:
Afforestation
Vegetation greening
Hydrological effect
Macro-scale hydrological modeling
Three-North region of China

ABSTRACT

China has implemented a few large-scale afforestation programs in the arid and semi-arid areas, including the north-eastern, northern, and north-western regions, collectively referred to as the Three-North region (TNR), to combat desertification and control dust storms. Although these programs have alleviated environmental problems in the region to a certain extent, the effects of increasing vegetation greenness on the hydrological cycle remain controversial. In this study, the relative effects of afforestation programs on the hydrologic processes in the TNR were identified based on large-scale hydrological modeling and satellite remote sensing data. The model forcing was featured with long-term vegetation dynamics. The study period ranged from 2000 to 2015, during which the greening of vegetation in the TNR was increased after multiple afforestation programs were carried out around 2000. The results indicated that, despite the spatial heterogeneity, the vegetation leaf area index (LAI) exhibited a significant increase across the TNR. Evapotranspiration (ET) increased over the entire region at the rate of 2.9 mm/year from 2000 to 2015, and its spatial pattern was consistent with changes in the LAI and precipitation. However, this does not imply equal contribution by vegetation growth and precipitation change. The results from the simulation scenarios indicated that precipitation change had a more significant influence on the ET, soil moisture and runoff than vegetation growth at the regional scale. Vegetation greening and precipitation increase in the Loess Plateau indicated their approximately equal impacts on ET and soil moisture. Consequently, the hydrological cycle was sensitive to afforestation practices at small-catchment or sub-regional scales where the magnitude of vegetation greening is relatively high. Therefore, the hydrological effect of vegetation greening at large scale may be overestimated by previous studies. To ensure sustainable water resource management at the TNR scale, special attention should be paid to climate change rather than afforestation efforts under the current level of ecological restoration programs.

1. Introduction

The arid and semi-arid areas in China have experienced serious ecological and environmental problems which have restricted sustainable socio-economic development (Duan et al., 2011; Zhang et al., 2016b; Zhu et al., 2017). Afforestation or reforestation is generally effective in improving environmental conditions and may have substantial impacts on the hydrological cycle by increasing rainfall interception and transpiration (Buendia et al., 2016; Peel et al., 2010). China has implemented some large-scale ecological restoration programs (e.g., the Three-North Forest Shelterbelt (TNFS) program) in the arid and semi-arid terrestrial areas since 1978, to significantly improve the ecological environment in the Three-North region (TNR) (Wang et al., 2010; Zhu et al., 2017). The project goal is to expect an increase in the forest coverage in arid and semi-arid China from 5% to 15% by 2050 (Liu et al., 2013). Therefore, given their long-term nature and importance in alleviating environmental issues, such programs require detailed and systemic evaluation on hydrological effect (Cao et al., 2011; Duan et al., 2011; Piao et al., 2015; Wang et al., 2010). Moreover, there is an urgent need to understand the effects of the vegetation greening on the local eco-hydrological environment because the implementation of many follow-up ecological projects around 2000 has led to the gradual increase of afforestation (Chen et al., 2019; Feng et al., 2016; Liu et al., 2014).

Large-scale afforestation can alter the water balance by regulating water cycle and energy cycle processes (Bonan, 2008). Although the

* Corresponding author.
E-mail address: xianhong@bnu.edu.cn (X. Xie).

https://doi.org/10.1016/j.jhydrol.2020.125689

Available online 2 November 2020
0022-1694/© 2020 The Authors. Published by Elsevier B.V. This is an open access article under the CC BY-NC-ND license (http://creativecommons.org/licenses/by-nc-nd/4.0/).

TNFS program eased environmental problems in the region to some extent, the consequences of large-scale afforestation on the hydrological cycles are still contentious (Liu et al., 2016). It is generally accepted that vegetation exhibits a water conservation function by retaining moisture through the root system (Zhang et al., 2011, 2016a). However, despite the greater retention of precipitation, more water is required to sustain the newly planted ecosystem. An increase in vegetation will likely promote evapotranspiration (ET), thus, reducing the availability of water for runoff and soil moisture (Feng et al., 2016).

In the context of global climate change, the changes in hydrological cycles and their relationship with climatic factors cannot be ignored because this region is highly sensitive to climate change (Yao et al., 2019; Zhu et al., 2020). The hydrological cycle is influenced by various climatic factors such as solar radiation, wind speed, precipitation, relative humidity, and air temperatures (Wang et al., 2017). There are significant spatio-temporal diversities in the dominant climatic factors that reshape the hydrological cycle due to the climate-vegetation-water interactions, especially those in the Loess Plateau region (Ma et al., 2008; Wang et al., 2017; Zhang et al., 2015a).

Given the complex environment characterized by ecological restoration and climate change, it is critical to elucidate the major factors that drive changes in the hydrological cycle in the TNR. A comprehensive understanding of this issue is important for integrated water resources management to ensure sustainable utilization of water resources (Bao et al., 2012; Feng et al., 2016). Several studies have attempted to quantify the effects of afforestation and climate change on the hydrological cycle (Gao et al., 2016; Herron et al., 2002; Xie et al., 2015). However, understanding the interactions among hydrological systems, vegetation, and climate factors is still limited (Bonan, 2008; Gerten et al., 2004; Rodriguez-Iturbe et al., 2007). A number of attribution analyses regarding hydrological variations in the TNR suggested climate variability and land-cover change to be the major factors driving streamflow in different sub-basins (Bao et al., 2012; Xie et al., 2015; Zhang et al., 2015b). Considering the differences among previous studies with regard to the study area and the time period, we suspect the magnitude of climate and vegetation dynamics in different periods may be one of the reasons for the debate.

The hydrological effects of afforestation or reforestation with regard to the ET and runoff may vary with scales. In particular, there is consensus regarding the hydrological response of small watersheds to afforestation (Zhang et al., 2017a). Specifically, ecological restoration was found to increase ET and simultaneously decrease water yield locally, while the degradation of vegetation indicated the opposite effect (Andréassian, 2004; Bruijnzeel, 2004; Liu et al., 2016). However, the hydrological effects of afforestation at large river basin and regional scales may be inconsistent (Li et al., 2017; Liu et al., 2016). The uncertainty in this regard for large watersheds (>10,000 ha) can be attributed to the complexity in watershed processes and the diversity of environmental conditions and land cover changes (Moore and Wondzell, 2005; Vose et al., 2011; Wei et al., 2003). Since the geographical area of the TNR is approximately 5.3 million km^2 and spans varying climatic conditions and land covers, it is necessary to conduct detailed studies on the hydrological impacts of afforestation.

The objective of this study was to evaluate the impacts of afforestation and climate change on the hydrological cycle at the regional scale based on remote sensing products and a large-scale land surface hydrological model, i.e., the Variable Infiltration Capacity (VIC) model. This study focused on the time period from 2000 to 2015 when the vegetation growth stage in the TNR was increasing sharply because of afforestation activities around the year of 2000 (Liu et al., 2014). To quantify the influence of different factors, the long-term dynamic vegetation growth index, also known as the leaf area index (LAI), and gridded atmospheric data were incorporated into the VIC model. LAI is an important parameter to simulate terrestrial ecological process as well as water, energy flux, and biogeochemical cycles, considering it as a crucial variable related to moisture conditions in the VIC model (Bohn and Vivoni, 2015; Fang et al., 2003).

2. Study area and data

2.1. Study area

The TNR of China ranges from 73.57° E to 134.57° E and from 32.23° N to 53.54° N (Fig. 1a) and contains arid, semi-arid, and humid areas. It covers an area of approximately 5.3 million km^2 and consists of five large river basins: the Songhua River (SR), Liao River (LR), Hai River (HR), Yellow River (YR), and the Inland River (IR) basins. The TNR was selected as the study site because several afforestation projects have been carried out in this region since the end of the 20th century including the TNFS, the Grain to Green Program, and the Natural Forest Protection Program (Feng et al., 2013; Xu et al., 2006). The vegetation cover increased due to the implementation of afforestation projects and the warmer climatic conditions (Xie et al., 2015).

The TNR was characterized by temperate monsoon and temperate continental climatic conditions. Owing to its large geographic area, the mean annual precipitation in this region varied greatly and was affected by the monsoon. Rainfall decreased from southeast (>1,100 mm) to the northwest (<50 mm). The mean annual temperature of the THR was diverse and ranged from 17 °C in the south to less than 0 °C in the north. Therefore, the vegetation was mainly distributed in the northeast and southern TNR in accordance with the climatic conditions. The northwest TNR was mainly grassland and desert.

To determine the hydrological effects of vegetation growth at the sub-region scale, two typical afforestation areas were selected for further study: the Horqin Sand Land and the Loess Plateau (Fig. 1b). The Horqin Sand Land (118.5° E to 124.3° E, 42.5° N to 44.8° N) is situated in the LR basin and the annual mean precipitation in this region for 2000–2015 was about 380 mm while the annual mean temperature was 6.7 °C. The landscape is characterized by dunes facing serious land degradation and desertification problems (Zhao et al., 2007). Moreover, this region is selected as it is also a typical low shrub afforestation region (Liu et al., 2011). The second sub-regional scale area is located in the Loess Plateau (107° E to 112.5° E, 35° N to 40° N) of the YR basin. This region is characterized by a semi-arid continental monsoon. For 2000–2015, the annual mean precipitation was 470 mm and the annual mean temperature was 9.4 °C. Intensive industrial and agricultural practices in the past decades have caused serious soil erosion in this region. To alleviate the soil erosion, a large area of the crop land in the Loess Plateau was converted to forest or grassland under the Grain for Green Program (Feng et al., 2016). Overall, the two sub-regions are characterized by distinct land cover types, i.e., low shrub and mixed forest, respectively.

2.2. Data

The VIC model required data include atmospheric forcing, soil, and vegetation. The atmospheric forcing dataset included daily precipitation, maximum and minimum temperature, and wind speed values from 1995 to 2015. These gridded atmospheric datasets, with a spatial resolution of 0.25°, were generated using the linear interpolation method with observations from 2,483 stations which were obtained from the China Meteorological Administration (CMA, http://data.cma.cn/) (Xie et al., 2015). Data for soil parameters for each grid cells, such as porosity, variable infiltration curve, and saturated hydraulic conductivity, were originally sourced from global soil datasets (Nijssen et al., 2001). These data have been successfully evaluated (Xie et al., 2015), and a further evaluation of these is presented in the next section.

Vegetation datasets included classification and corresponding vegetation parameters. Vegetation classification data were derived from land cover maps for the year 2005 produced with Landsat TM images (Liu et al., 2010). Previous studies have demonstrated the suitable quality of these data (Liu et al., 2010; Xie et al., 2015). All vegetation parameters, except LAI, were obtained from Xie et al. (2015). The LAI data from

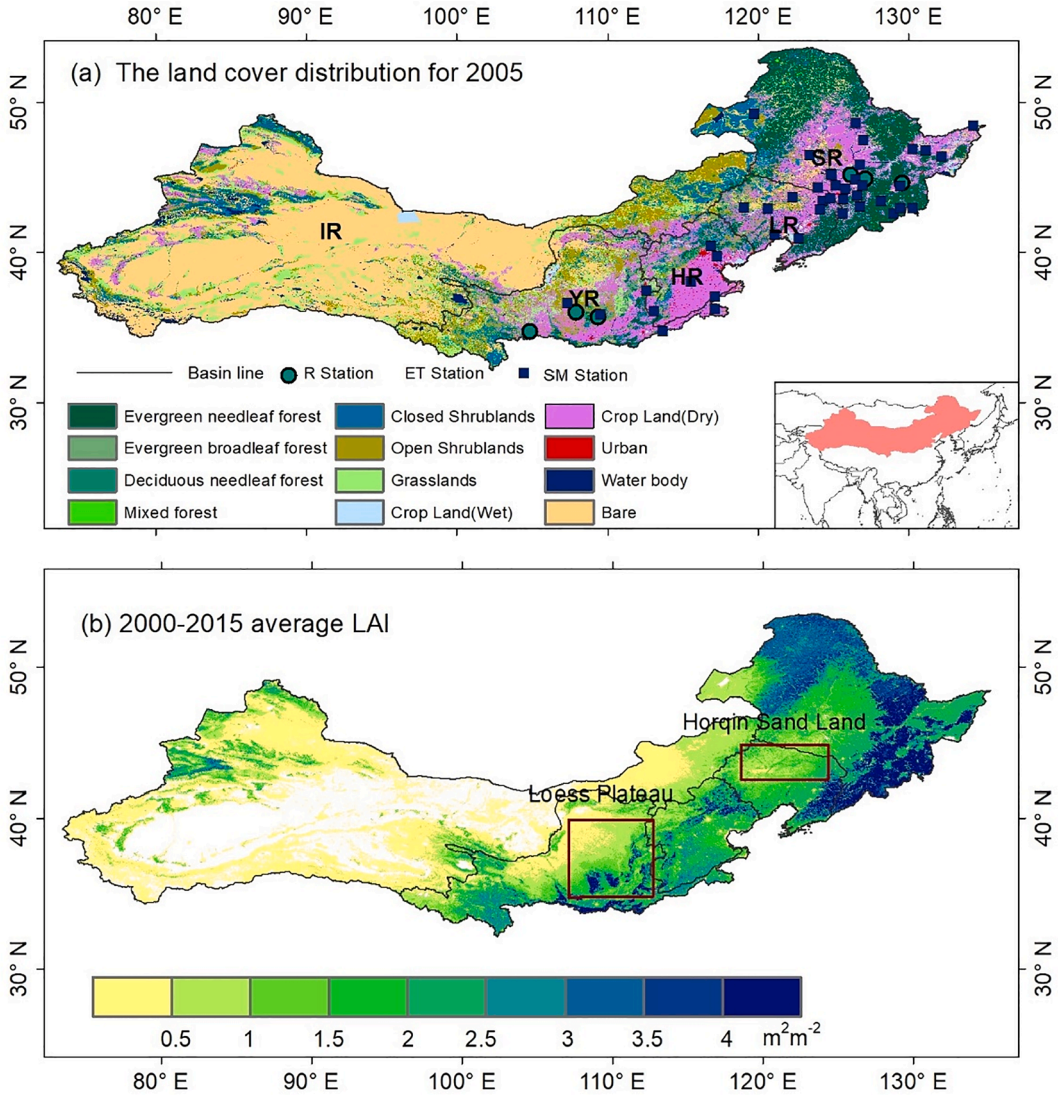

Fig. 1. (a) Location of the Three-North region (TNR) with land cover distribution in five large river basins: Songhuajiang River (SR), Liao River (LR), Hai River (HR), Yellow River (YR), and Inland River (IR) in 2005; (b) The average leaf area index (LAI) for the growing season from 2000 to 2015.

2000 to 2015, used as the forcing input in this study, were obtained from the eight-day composite Global Land Surface Satellite (GLASS) product with a spatial resolution of 1-km. The GLASS LAI product was retrieved from the Moderate Resolution Imaging Spectroradiometer reflectance data (MOD09A1) using the general regression neural networks algorithm (Xiao et al., 2014, 2016). An important advantage of GLASS LAI is solving the problem of information missing by using multi-temporal data and preprocessing input data (Ma et al., 2017; Xiao et al., 2015). A number of studies have indicated that GLASS LAI is suitable to represent vegetation dynamics in China (Guli et al., 2015; Ma et al., 2017; Piao et al., 2015). To adapt to simulations with the VIC model, the 1-km and eight-day composite LAI data were linearly interpolated to daily resolution for each land cover type in each grid cell and set up as input forcing data.

To evaluate the VIC performance for soil moisture simulation, the combined active/passive soil moisture product developed by the European Space Agency (ESA) under the Climate Change Initiative (CCI) (http://www.esa-soilmoisture-cci.org) was obtained (Dorigo et al., 2017; Gruber et al., 2017). This remote sensing soil moisture product (referred to as ESA-CCI SM hereafter) has been extensively evaluated and widely used under different environmental conditions (González-Zamora et al., 2018; Karthikeyan et al., 2017a, 2017b). The combined products used in this study spanned over a period ranging from 2000 to 2015 and had a spatial resolution of 0.25°.

Moreover, the evaluation about VIC simulated ET was conducted by remote sensing products from the Global Land Evaporation Amsterdam Model (GLEAM) (https://www.gleam.eu/) (Martens et al., 2017; Miralles et al., 2011). The GLEAM algorithms maximized the recovery of terrestrial evaporation information by estimating all components of daily ET based on satellite observations separately. The product has a spatial resolution of 0.25° and temporal resolutions of daily, monthly and yearly dimensions. GLEAM ET has been well evaluated and widely used (Yang et al., 2017, 2018), therefore monthly GLEAM ET data were used in this study for the period from 2000 to 2015.

Besides the remote sensing data, in-situ soil moisture observations from 43 stations, ET observations from 16 flux towers and streamflow observations from six hydrological stations were obtained to evaluate the model performance. The in-situ soil moisture observations were obtained from the CMA for the period of 2000 to 2014. The observed depth was 100 cm with a sampling interval of 10 days. The ET observations were collected under a Coordinated Enhanced Observation Project (CEOP) in arid and semi-arid regions of northern China (Jia et al., 2012; Xie et al., 2015). The observation locations and time periods were shown in Table 1. The monthly streamflow data were from the

Table 1
ET flux measurement stations and statistical metrics (Pearson correlation coefficient r, Relative bias (Bias) and Relative root mean square error (RRMSE) used to evaluate the VIC performance.

Station	Latitude	Longitude	Period (Year)	r	Bias (%)	RRMSE (%)
Changbaishan	42.40	128.10	2002–2007	0.79	15.89	55.36
Laoshan	45.28	127.58	2003–2007	0.73	−4.83	73.27
Jinzhou	41.18	121.21	2008–2009	0.75	15.99	38.01
Neiman	42.93	121.70	2008	0.86	8.65	28.12
Yucheng	36.83	116.57	2002–2007	0.77	20.20	57.20
Duolun	42.05	116.67	2006	0.84	32.02	63.09
Arou	38.05	100.46	2012–2015	0.91	15.37	38.59
Changwu	35.25	107.68	2008–2009	0.86	−0.43	33.45
Kubuqi	40.54	108.69	2006	0.85	21.47	49.02
Shapotou	37.53	105.80	2009	0.92	19.92	39.28
Yuzhong	35.95	104.13	2008–2009	0.66	12.81	51.58
Dingxi	35.56	104.59	2008	0.57	12.2	46.83
Maqu	33.89	102.14	2009	0.62	8.28	29.41
Baijitan	38.92	100.30	2012–2013	0.81	−10.38	94.49
Huzhaizi	38.77	100.32	2012–2015	0.71	−8.32	66.62
Haibei	37.62	101.32	2002–2007	0.84	19.71	54.69

Annual Hydrological Report for P. R. China during 2000–2015 period. Considering the scale difference between the in-situ observations (soil moisture and ET) and model simulation, the observation stations were selected within 5 km from the center of the grid for comparison. The VIC simulated soil moisture and ET were assumed comparable with the in-situ observations, as the daily atmospheric forcing dataset for the VIC model were interpolated according to the location of each grid center.

3. Methods

3.1. Macro-scale hydrological model

The VIC model was used to assess the impacts of climate and vegetation dynamics on the hydrologic processes in the TNR. The VIC model is a widely used macro-scale land surface hydrological model (Liang et al., 1994, 1996) which can simulate water and energy interactions within the soil, vegetation, and the atmosphere (Nijssen et al., 2001; Wang et al., 2012; Xie et al., 2015, 2020). The VIC model divides the study area into multiple uniform grid cells and outputs water and energy states and fluxes for each grid cell. It characterizes sub-grid spatial variability with regard to the topography and vegetation/land cover. Canopy interception storage, infiltration, surface runoff, subsurface runoff, ET, and energy fluxes are simulated at the sub-grid scale. The output ET and runoff of are sums of all sub-grid results according to the weight of the area. ET includes evaporation of canopy interception, soil evaporation, and plant transpiration (Bohn and Vivoni, 2015). The soil column of each grid cell is generally divided into (but not limited to) three layers to represent the dynamic response of water and energy to the atmospheric and land surface forcing. Total runoff of each grid cell includes surface runoff and base flow. The surface runoff is generated in the upper two layers based on principles of infiltration and excess storage. The subsurface runoff is simulated from the bottom soil layers based on the ARNO model. Subsequently, the routing model can be used to transform the runoff of each grid into stream flow for a given basin.

3.2. Model setup and experimental design

To investigate the hydrological effects of climate change and vegetation growth in the TNR from 2000 to 2015, four simulation scenarios were designed: baseline, precipitation-detrend, temperature-detrend, and LAI-detrend. For the baseline scenario, the model used the original daily atmospheric and LAI forcing data as well as the soil and vegetation parameters mentioned above. The model was run for 1995–2015. The datasets for the first 5 years were used to spin the model and the simulations for the remaining 16 years were used to analyze the variabilities of hydrological variables. As the LAI data were available from the year 2000, the 5-year spinning-up simulation employed an average LAI computed from 2000 to 2003. The simulation under this scenario was referred to as the control-run or baseline simulation.

With regard to the precipitation-detrend simulation scenario, the long-term precipitation trends were linearly removed, and the other forcing variables were kept as the baseline simulation scenario.

$$P'_{Y_{i,d}} = \left[\frac{P_{Y_i} + a^*(Y_b - Y_i)}{P_{Y_i}}\right] * P_{Y_{i,d}} \quad (1)$$

where, $P'_{Y_{i,d}}$ denotes the daily detrended precipitation on day d in the year Y_i; $P_{Y_{i,d}}$ is the original daily precipitation; P_{Y_i} refers to the annual precipitation in the year Y_i; Y_i represents years from 2000 to 2015, Y_b is the reference year 2000; and a is the linear trend of annual precipitation.

For the temperature-detrend simulation scenario, the daily maximum and minimum temperature data were linearly detrended using Eq. (2).

$$T'_{Y_{i,d}} = T_{Y_{i,d}} + b(Y_b - Y_i) \quad (2)$$

where, $T'_{Y_{i,d}}$ and $T_{Y_{i,d}}$ are the detrended and original daily temperatures, respectively; b is the linear trend of the annual average temperature. In both simulation scenarios, the linear trend for either the annual precipitation or the average temperature was removed and the seasonal dynamics were kept.

For the LAI-detrend scenario, the daily average LAI was computed from 2000 to 2003 time period to replace the original LAI forcing computed from 2000 to 2015 time period. This approach not only removed the changing trend but also effectively avoided the uncertainties due to abrupt land cover changes in a given year.

Comparisons among the four simulation scenarios were designed to examine the effects of changes in climatic factors or vegetation greenness on the hydrological cycle. The difference between the baseline and detrended scenarios with regard to the ET and soil moisture were evaluated to allow subsequent quantification of the magnitude of change caused by different factors at the basin scale.

4. Results

4.1. Model evaluation

Prior to applying modeling for the above-mentioned scenarios, the VIC model was evaluated for its suitability to simulate the hydrological processes in the TNR. While the former has been successfully evaluated by Xie et al. (2015) using streamflow from 16 gauges and ET from 10 stations, we validated it further—as mentioned in Section 2.2—using remote sensing products and in-situ observations.

4.1.1. Soil moisture validation

The VIC simulated soil moisture was validated using the ESA-CCI SM. Although the ESA-CCI SM has been applied widely (An et al., 2016; Chakravorty et al., 2016; Peng et al., 2015; Shen et al., 2016), it cannot disregard missing data for some regions and the differences in sensing depths between the satellite (<5 cm) and model simulations (>10 cm) (An et al., 2016). However, this product could be compared to the soil moisture in the top layer as simulated by the VIC model. Fig. 2a and b indicate the long-term average soil moisture simulated by the VIC model and the ESA-CCI from 2000 to 2015. Spatial differences notwithstanding, the VIC model and the ESA-CCI product provided close estimates for the long-term average soil moisture, i.e., 20.19 mm and 19.31 mm, respectively. The results indicated that soil moisture gradually decreased from the southeast to the northwest and the SR basin had the highest soil moisture value. Moreover, the VIC model and the ESA-CCI provided similar variations for the annual soil moisture (Fig. 2c) and the seasonal cycle (Fig. 2d). The VIC model presented slightly higher soil moisture estimates than the ESA-CCI. This small difference was partly because the ESA-CCI only monitored soil moisture in the top-thin layer and had missing data for winter.

As remote sensing satellites can only detect top-thin surface soil moisture, a total of 43 sites of soil moisture observations were selected to validate the deep-depth VIC simulations. The in-situ soil moisture data were sampled at a 10-day interval; therefore, the Pearson correlation coefficient (r) and relative bias (Bias) were calculated. Fig. 3 shows the two metrics for the 43 observation sites. The relative bias ranged from −20% to 20% for the deep soil moisture. The r values for most stations were greater than 0.8 and the highest reached 0.98. Despite discrepancies in the spatial scales of observed and simulated soil moisture, the VIC generally provided acceptable estimates of soil moisture in the deep layers. These results demonstrated that the VIC model was suitable for simulating the soil moisture in the TNR.

4.1.2. ET validation

The VIC ET was evaluated using the remote sensing product and the in-situ observations. Fig. 4a and b indicate the long-term average ET in the growing season (April to September) simulated by the VIC model and the GLEAM data from 2000 to 2015. In general, the spatial distribution patterns of the two ET products were consistent, decreasing from the southeast to the northwest of the study area. These two ET products

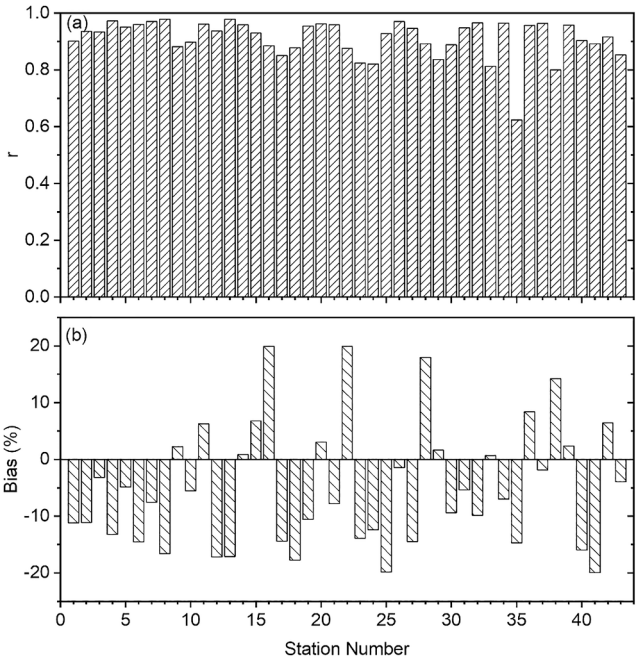

Fig. 3. Pearson correlation coefficient (r) and relative bias (Bias) between the observed and the simulated soil moisture (about 100 cm deep) at the 43 stations shown in Fig. 1.

were slightly different in some regions, which may be due to the sparse distribution of observation sites for atmospheric forcing interpolation in these regions. The GLEAM ET product is significantly overestimated in the northern region of the SR basin compared with the VIC simulation, because the average ET of some grids is higher than the average precipitation. Moreover, the r value for each grid (Fig. 4c) was calculated according to the monthly ETs in the growing season as determined by the two products. In the desert region of the IR basin, the correlation coefficient between the two products was less than 0.5 due to the lack of precipitation and irregular distribution during the year. However, although there was sparse vegetation cover in this region, that was not the focus of this study. Apart from this region, the correlation

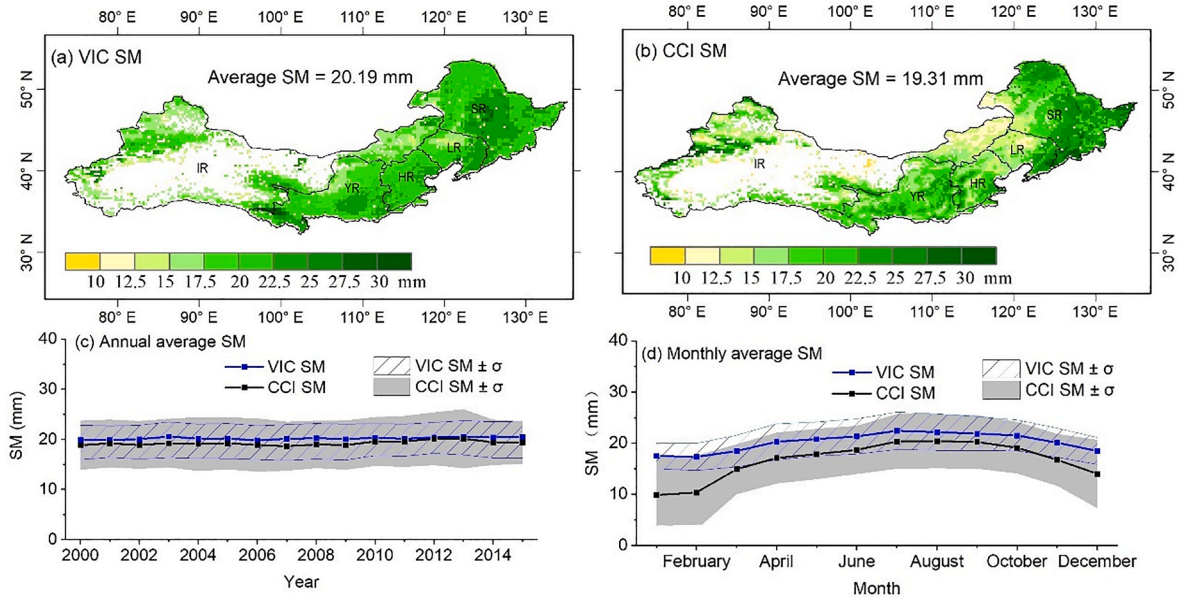

Fig. 2. Soil moisture (SM) estimated from the VIC model and ESA-CCI: (a) Long-term average SM from the VIC simulation; (b) Long-term average SM from the ESA-CCI; (c) Annual SM from the VIC and ESA-CCI; and (d) Seasonal SM from the VIC and ESA-CCI.

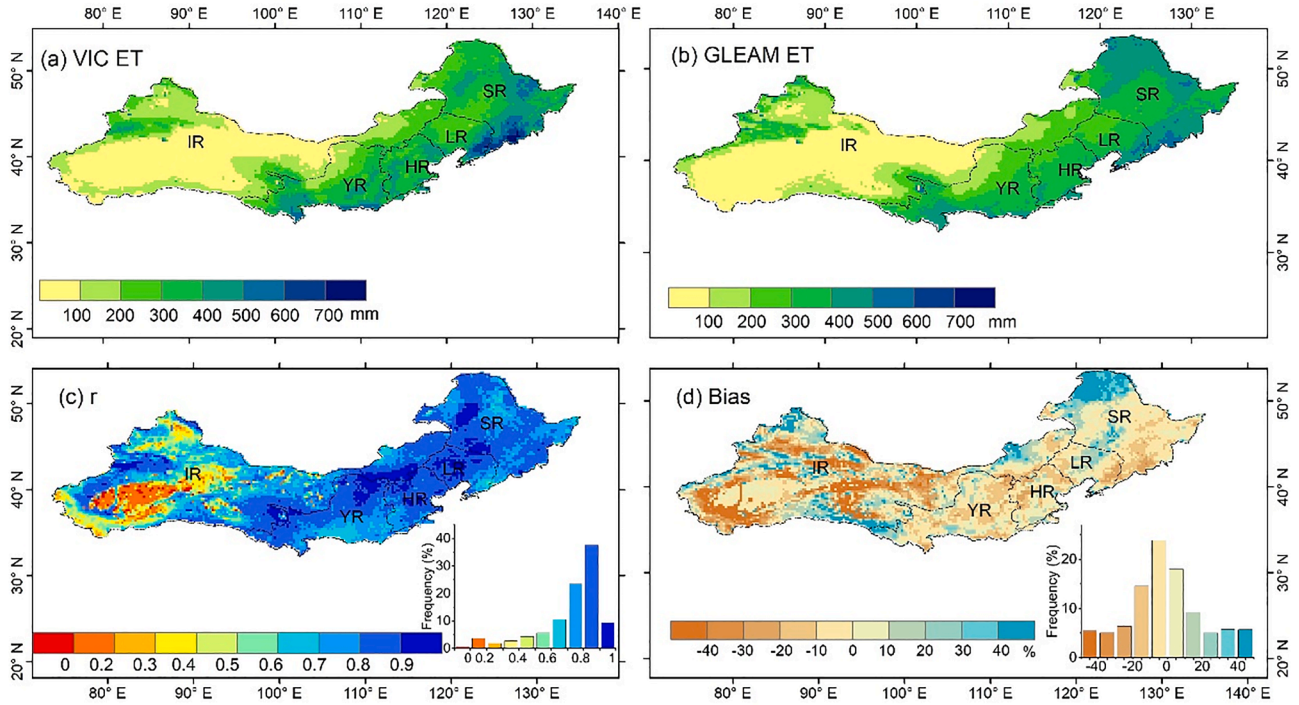

Fig. 4. Evapotranspiration (ET) in growing seasons estimated from the VIC model and GLEAM: (a) Long-term average ET from the VIC model; (b) Long-term average ET from the GLEAM; (c) Pearson correlation coefficient (r) between the two monthly ET serials; and (d) Bias between the two average ETs.

coefficients on the grids were greater than 0.6 and even up to 0.9 in some areas. Fig. 4d shows the bias between the two long-term average ETs. Except for the areas with large differences mentioned earlier, the bias ranged from −30% to 30% for the average ET. Although the values of the two data sets vary slightly, the results indicated that evapotranspiration of the VIC simulation was reasonable for the spatial distribution.

Besides comparing spatial distributions between the two datasets, the reliability of ET within the time variation was also validated. Fig. 5 exhibits the monthly ET of the VIC model and GLEAM in the five basin scales. The results show that the simulations capture the GLEAM ET evolutions and magnitudes reasonably well for the monthly-scale time series, although there were a few differences in April. The statistical

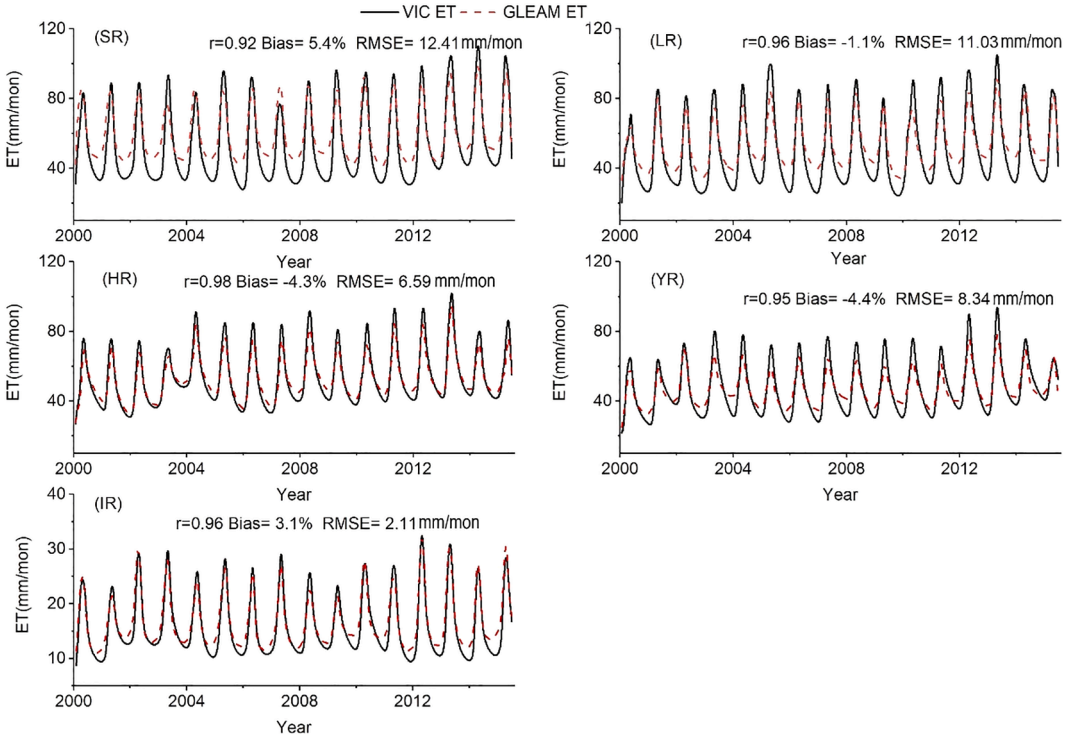

Fig. 5. Simulated monthly ET against GLEAM ET for the growing season in the five basins: Songhuajiang River (SR), Liao River (LR), Hai River (HR), Yellow River (YR), and Inland River (IR).

indices also indicate that the results were reliable. Their absolute relative biases are less than 5%, except for that of the SR basin (5.4%), which was due mainly to the VIC model underestimations of the ET in April. The root-mean-square errors (RMSE) were less than 10 mm/month except for the SR and the LR basins. However, the results were acceptable for long-term ET simulations in the large basin scales.

The performance of the ET simulation was also evaluated with flux tower measurements. The metrics of r, Bias and relative root mean square error (RRMSE) are presented in Table 1. The r values were all greater than 0.6, with the exception of Dingxi station (r = 0.57). The simulated ET was slightly lower than the observed with most of the absolute Biases being less than 30%, mainly because of underestimation of ET in winter. Despite the relatively large RRMSEs, favorable agreements were achieved between the in-situ observations and the VIC simulated ET.

4.1.3. Streamflow validation

The VIC simulated streamflow was evaluated by observation data from the six hydrological stations. There will inevitably be some uncertainties in the simulation results, because the VIC model used in the study does not describe the impact of the other human activities (e.g., water withdrawal). However, the consistency of the simulated and the observed streamflow indicated that the VIC model generally performs acceptably for each catchment (Fig. 6). The Nash-Sutcliffe efficiencies (NSEs) of five stations were over 0.5. Despite the NSE of the Jiaokouhe station being only 0.27, the simulated streamflow could still roughly capture the peak flow. The r values were greater than or equal to 0.75. Therefore, the VIC model showed admissible performance for hydrological simulations in this region.

4.2. Climate and vegetation dynamics

4.2.1. Changes in precipitation and temperature

According to previous studies, precipitation and temperature are the influential climatic forcing factors that affect the hydrological cycle (Li et al., 2018; Xie et al., 2015). Therefore, first, the interannual trends of precipitation and temperature were detected with the Mann-Kendall method which is commonly used in hydrology and meteorology (Gocic and Trajkovic, 2013; Hamed, 2008). The annual precipitation exhibited high spatial heterogeneity and increased in most of the TNR from 2000 to 2015 (Fig. 7a). The areas with obvious increase in precipitation were mainly located throughout the entire SR basin (9.73 mm/year), within the southeastern LR basin (7.90 mm/year), most of the HR basin (5.58 mm/year), and the eastern and southern parts of the YR basin (5.32 mm/year). Precipitation in the IR basin mainly showed a downward trend. Despite the fluctuation, precipitation presented a substantial increase across the TNR at a rate of 3.96 mm/year from 2000 to 2015 (Fig. 7c).

Throughout the TNR, the mean temperature did not change significantly suggesting that its influence on hydrological cycle may not be obvious (Fig. 7b); however, despite spatial differences, a slight positive increase appears in most areas. A small section in the southwestern YR basin presents a significant temperature increase with a rate of more than 0.06 °C. The temperatures in some parts of the SR basin and the western region of the IR basin decreased during the last decade. Therefore, temperature does not show obvious trends at the regional scale in the TNR from 2000 to 2015 (Fig. 7d).

4.2.2. Changes in the LAI

The trends in vegetation greenness during the growing season (April to September) were examined from 2000 to 2015 using the GLASS LAI (Fig. 8). Results indicate that LAI increased substantially over the TNR. The areas with significant increase (>0.01 m^2 m^{-2} $year^{-1}$) and slightly

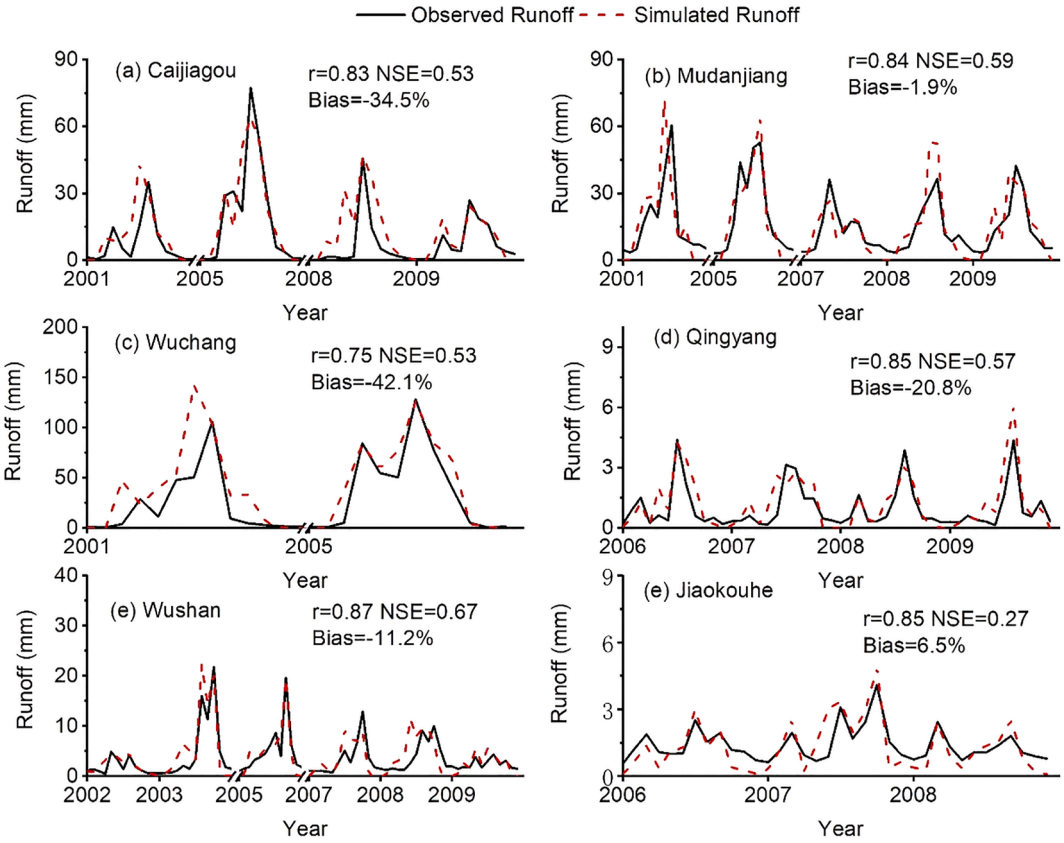

Fig. 6. Simulated monthly streamflow against observations for the whole year from six gauges.

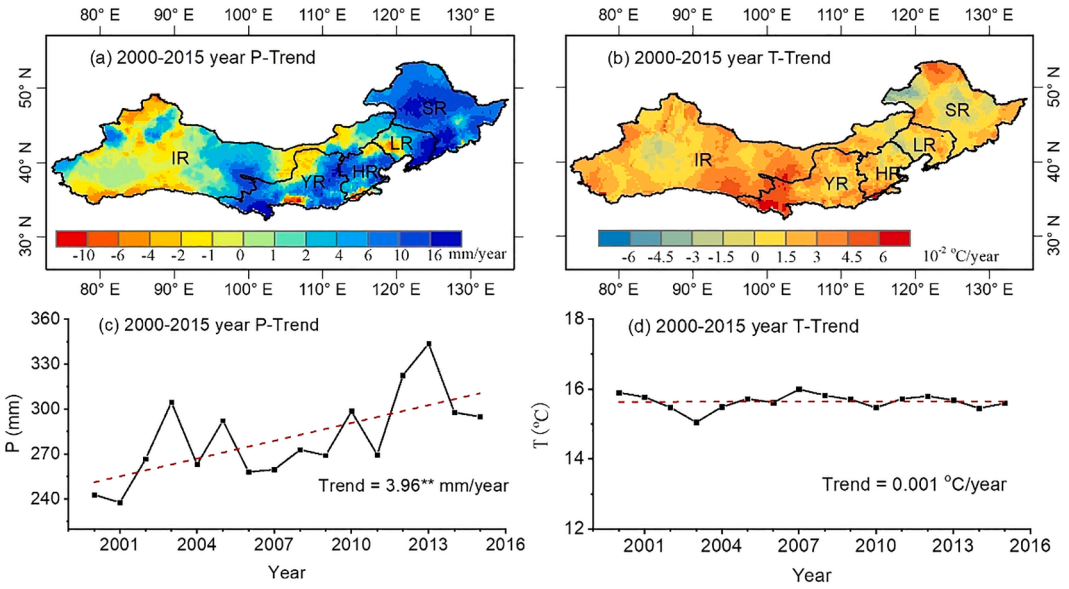

Fig. 7. Precipitation (left) and temperature (right) changes in the TNR from 2000 to 2015. The asterisk (**) indicates statistically significant trends at $p < 0.05$.

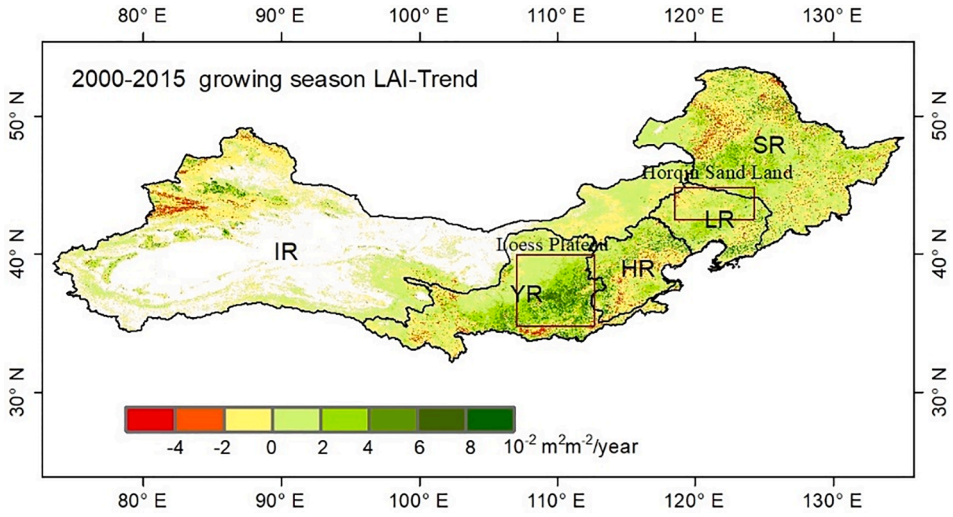

Fig. 8. Trends of vegetation greenness as characterized by LAI for the TNR from 2000 to 2015. The white color indicates no LAI data available.

increase (0.001–0.01 $m^2\ m^{-2}\ year^{-1}$) account for 25.04% and 21.67% of the TNR, respectively. The areas with significant increase were mainly distributed across the Loess Plateau in the YR basin, the northern HR basin, the central LR basin, and the southwestern SR basin. These results are consistent with those of another study focusing on the vegetation greenness in China (Liu et al., 2016). In addition to LAI, the remote sensing normalized difference vegetation index (NDVI), which was also used to represent greenness, also clearly increased in the Loess Plateau (Liu and Gong, 2012).

Despite the greening in most areas of the TNR, some areas experienced vegetation degradation, which was characterized by a decrease in the LAI. For example, vegetation degradation in the YR and HR basins may be attributed to the geographical expansion of urban and farmlands. With regard to the SR basin, the land use conversion from woodland to grassland might have contributed to the decreasing LAI (Liu et al., 2012a, 2010; Ning et al., 2015).

The vegetation greenness in the growing season exhibited high spatial variability for the period 2000–2015 (Fig. 9) due to the impact of climate change and land use transitions. The vegetation greenness in the Loess Plateau increased with a rate of up to 0.0148 $m^2\ m^{-2}\ year^{-1}$ because of the Grain for Green Project, which has been implemented since 1999 (Feng et al., 2016; Liu et al., 2008; Wang et al., 2015). The increase in LAI in the HR and LR basins (characterized by suitable growing conditions for vegetation) reached 0.0116 $m^2\ m^{-2}\ year^{-1}$ and 0.012 $m^2\ m^{-2}\ year^{-1}$, respectively. The greening rate in the IR was relatively small because of water-limited conditions. Overall, the LAI indicated an increasing trend for the entire TNR for the period 2000–2015, without respect to the yearly variation.

4.3. Response of the ET

The response of the ET was analyzed as it is sensitive to climate and vegetation dynamics (Jung et al., 2010; Wang et al., 2017). Based on the simulation scenarios described in Section 3.2, daily ET was simulated for each scenario and the total ET was calculated for the growing season. Fig. 10a shows ET simulated from the baseline scenario. The areas with a positive trend occupied 72% of the TNR, and the remaining areas indicated a negative trend during the 16-year study period. Overall, the ET increased at the rate of 2.86 mm/year. The areas with significant increase (>5 mm/year), accounting for about a quarter of the entire TNR,

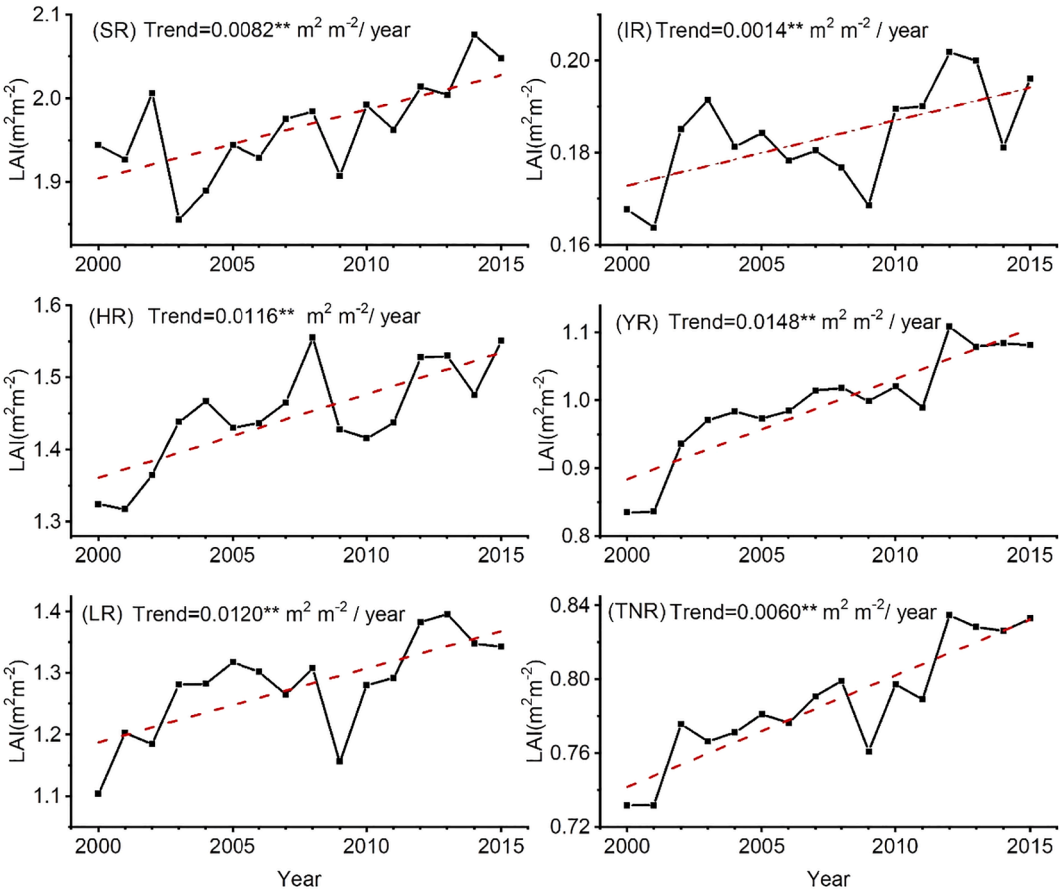

Fig. 9. The mean LAI during the growing season for each year in the five basins and for the entire TNR. The asterisk (**) indicates statistically significant trends at $p < 0.05$.

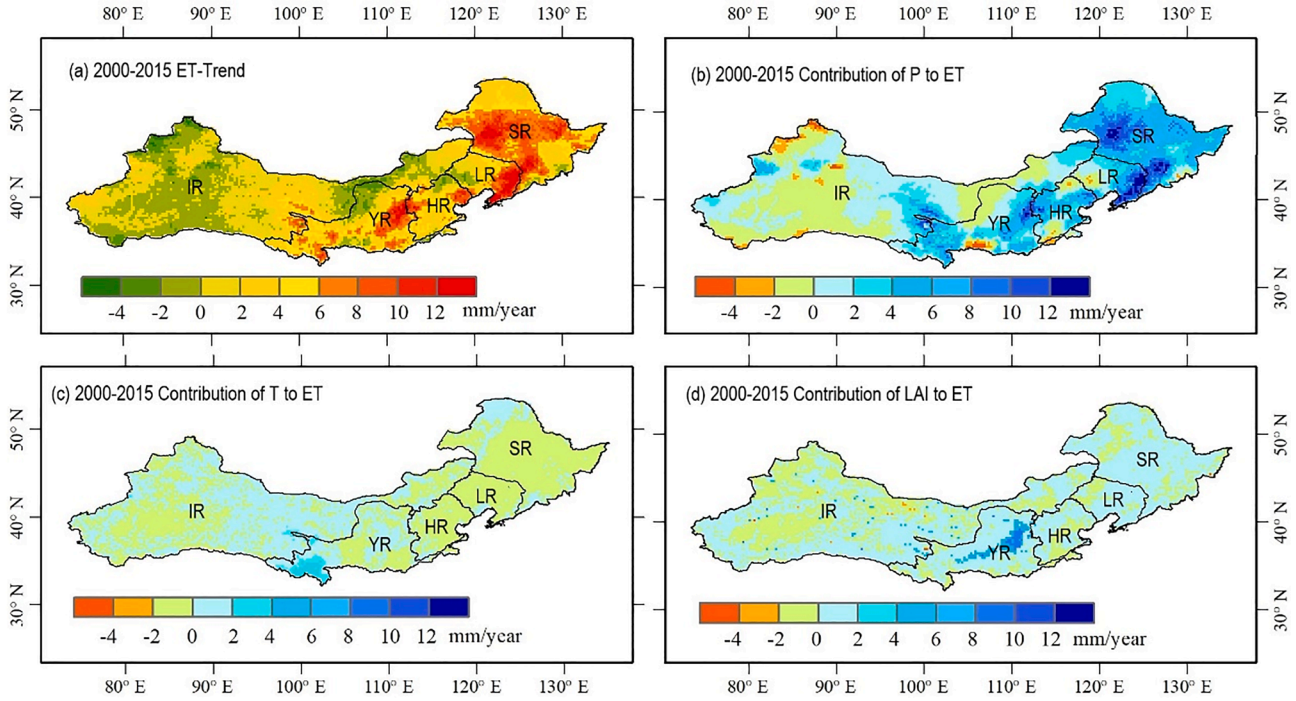

Fig. 10. (a) The trends in the ET. The other three plots indicate the influence of different driving forces in the TNR from 2000 to 2015: (b) Contribution of precipitation (P); (c) Contribution of temperatures (T); and (d) Contribution of LAI.

were mainly concentrated in areas of the SR basin, southeastern LR basin, parts of the Loess Plateau, and the southwestern YR basin. A slight decrease was observed in the IR basin. In contrast to the results presented in Fig. 7a and Fig. 8, the spatial pattern for ET was consistent with the changes in P and LAI. The ET generally increased in regions with positive precipitation and greening trends.

To identify the dominant factors driving ET variations, the differences between the baseline scenario and the three detrended scenarios with regard to the ET were calculated. Subsequently, the trends of the differences among the three scenarios were computed. In this regard, each trend was assumed to be contributed by one of the three environmental factors, i.e., precipitation, temperature, and vegetation (LAI).

As shown in Fig. 10b, c, and d, precipitation contributed to the largest ET increase, followed by vegetation and temperature. In the northeastern TNR, i.e., the SR basin in particular, precipitation enhanced the ET by about 91.41 mm in total over the 16 years (Table 2). The averaged ET increase over the entire TNR due to precipitation was up to 35.59 mm. Vegetation greening leaded to a relatively small ET increase in the entire TNR by nearly 4.82 mm. However, the ET increase in the YR basin due to vegetation greening reached 12.8 mm during the study period. Temperature had a negligible contribution to the increase or decrease in the five basins of the TNR.

4.4. Response of soil moisture

Changes in soil moisture showed complex spatial distributions (Fig. 11) and indicated a moderate average increase of 1.72 mm/year over the TNR, despite a slight decrease in the central and western parts of this region (i.e., the YR and the IR basins). Similar to the ET pattern, large positive trends for soil moisture were observed in most parts of the SR basin (3.13 mm/year) and the southeastern part of the LR basin. In contrast to the ET, the soil moisture in the whole YR basin decreased slightly, and increased in the southern part of the basin affected by precipitation change. Similarly, soil moisture presented substantial increasing trends in the southwestern IR basin, even greater than 6 mm/year in some areas. Other regions in the TNR indicated a slight upward or downward trend.

The complex changes in soil moisture can be explained by the drivers of climate and vegetation evolution. Similar to the ET analysis, their contributions to the soil moisture were quantified based on the four simulation scenarios. As shown in Table 2, changes in soil moisture were largely driven by variations in precipitation, which led to an average accumulated increase of about 20.85 mm across the TNR during the study period. In the eastern TNR (i.e., the SR basin), there was a precipitation-driven increase of up to 47.24 mm. A small increase or decrease in the soil moisture appeared in the IR basin; this was also primarily caused by the changing precipitation.

Vegetation growth, especially the survival of new plantations, needs to draw massive soil moisture. Vegetation greening contributed to the decrease in the soil moisture across the TNR with an accumulated decline of about 7.3 mm over the study period (Table 2). In particular, in the central area of the YR basin (i.e., the Loess Plateau), vegetation greening resulted in drier soils with a rate of about −4 mm/year. Compared to precipitation and vegetation, temperature had little impact on soil moisture dryness during the study period (Fig. 11c).

4.5. Hydrological response in typical afforestation regions

The above-mentioned results suggest that afforestation had a moderate effect on the hydrological cycle in the entire TNR at the basin scale. However, the hydrological cycle response to environmental changes displayed distinct spatial heterogeneity, implying that the hydrological effects of afforestation may be scale dependent (Gao et al., 2016; Zhang et al., 2017a). To identify the hydrological effects at smaller scales, two typical sub-regions, i.e., the Horqin Sand Land area and the Loess Plateau area, where intensive afforestation practices have been implemented, were selected for further analysis. As mentioned in Section 2.1, the two regions are characterized by distinct land cover types, i.e., low shrub and mixed forest, respectively. Our analysis is based on the simulation scenarios described in Section 3.2. Since the yearly temperature variation during the study period was very small for the two sub-regions, the temperature influence is not discussed in this section.

The Horqin Sand Land is an arid sub-region with an average LAI of 0.8 $m^2 m^{-2}$. The precipitation showed an upward trend (4.75 mm/year) along with a slightly increasing LAI (0.0079 $m^2 m^{-2} year^{-1}$) over the past 16 years (Fig. 12a). The precipitation and the LAI trends indicated a strong correlation in terms of their consistent temporal variations. Under the impact of the two competing factors, soil moisture in the Horqin Sand Land area continued to increase during the study period. In terms of the impact on the soil moisture dynamics, the precipitation displayed a positive contribution of up to 34.45 mm at 0–80 cm depth for the period, while LAI led to a negative effect about − 12.06 mm. With regard to ET, the response to LAI was negligible compared with the response to precipitation. These results suggest that the increase of the hydrological variables in the Horqin Sand Land area are attributable to precipitation and not afforestation.

The Loess Plateau is a semi-arid sub-region with higher precipitation and vegetation coverage. Its vegetation LAI also significantly increased from 0.7 to 1.2 $m^2 m^{-2}$. The increasing precipitation led to an increase in the soil moisture by about 27.07 mm (0–120 cm depth), and the increasing LAI caused the soil moisture to decline by about − 26.27 mm. The two factors induced an increase in the ET by 3.77 mm/year and 1.64 mm/year, respectively. Compared to the precipitation dominated Horqin Sand Land, vegetation almost equally impacted the soil moisture and the ET in the Loess Plateau. Therefore, the effects of afforestation practices on the hydrological cycle depended on the scale (i.e., the watershed area) of the study region and the magnitude of vegetation greening. Other studies have also supported this conclusion (Bi et al., 2014; Peel et al., 2010).

Table 2
Accumulated contributions of changes in precipitation (P), temperature (T), and the LAI to the ET, SM and R in the five basins and the entire TNR from 2000 to 2015.

	Contributor	SR	IR	HR	YR	LR	TNR
ET (mm)	P	91.41	−8.20	51.53	42.08	73.96	35.59
	T	−2.38	−1.20	−1.64	9.49	−1.71	1.50
	LAI	4.02	−2.85	4.06	12.80	4.67	4.82
SM (mm)	P	47.24	9.02	24.12	22.02	38.52	20.85
	T	1.10	−1.75	0.21	−2.74	0.64	−1.12
	LAI	−4.68	−5.85	−9.07	−13.84	−9.56	−7.30
R(mm)	P	19.57	0.72	11.82	5.31	18.99	7.36
	T	0.03	−0.11	0.19	0.54	0.01	−0.12
	LAI	−0.45	−0.06	−0.83	−0.92	−0.89	−0.37
P(mm)	changes	155.68	8.80	89.28	85.12	126.40	62.40

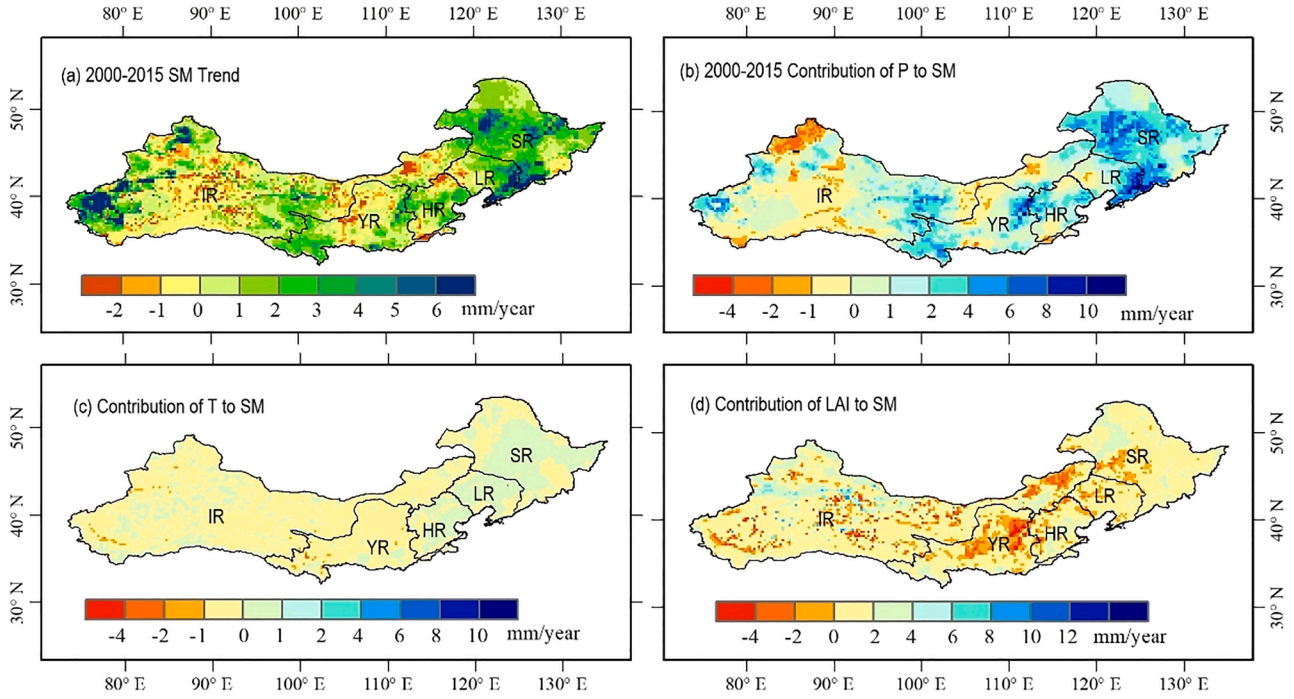

Fig. 11. (a) The trend in soil moisture. The other three plots indicate the influence of different driving forces in the TNR from 2000 to 2015; (b) Contribution of P; (c) Contribution of T; and (d) Contribution of LAI.

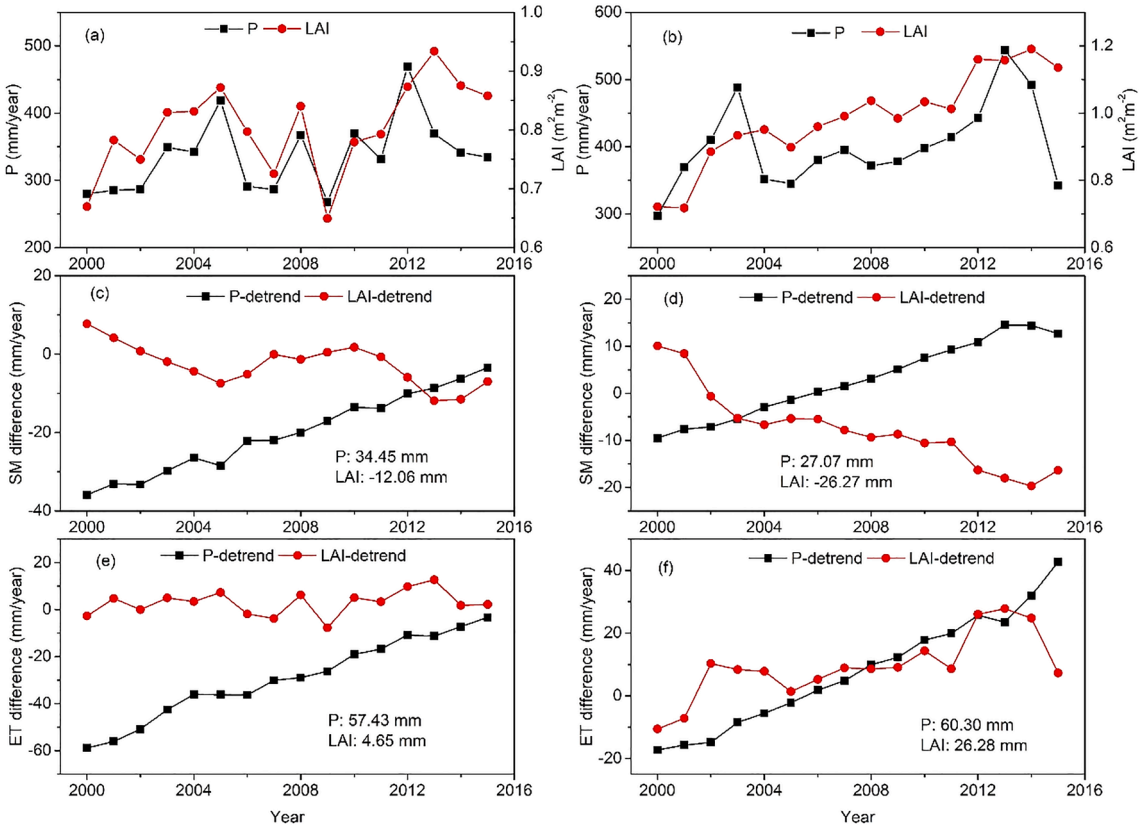

Fig. 12. Environmental changes and contributions to SM and ET at the Horqin Sand Land (left) and the Loess Plateau (right). The differences in plots c, d, e, and f were calculated from the two detrended scenarios minus the baseline scenario. The accumulated contribution of P and LAI are also presented in the four plots which were computed by multiplying the differences with the number of years (i.e., 16 years).

5. Discussion

5.1. Evolution of environment conditions

The results of this study indicated that except for the IR basin, precipitation in the TNR showed an upward trend from 2000 to 2015. Despite the spatial heterogeneity, the temperature change was negligible. A number of previous studies have also indirectly illustrated this pattern, in that the precipitation in the YR basin increased while temperature showed a slight downward trend from 2000 to 2012 (Zhang et al., 2015a), and temperature fluctuation in the northwest TNR was very small for the period 2000–2010 (Deng et al., 2014). Further, overall precipitation in the HR basin has been increasing since 2000 (Qin et al., 2015). There were slight differences in the magnitude of change with regard to climatic factors which may be affected by the size of the study area and the study period under consideration. The results of this study remain consistent with those of previous studies with regard to the overall trends of climate change.

Over the past three decades, vegetation greenness has increased in northern China due to factors such as afforestation, improvement of agricultural practices, and climatic warming (Duan et al., 2011; Liu et al., 2016; Piao et al., 2015). The LAI trends observed in this study indicate that the vegetation greenness in the TNR has increased during the growing season since 2000. This vegetation greening trend was also illustrated by other studies with different data sources (Liu and Gong, 2012; Liu et al., 2016). The vegetation greening can be caused by climate change, CO_2 fertilization, land cover change and other factors (Zhu et al., 2016). In this study area, the vegetation coverage rate increased due to the implementation of several ambitious programmes, and farmland management played an important role in the greening (Chen et al., 2019; Zhang et al., 2017b). Certainly, a wetting climate also promoted the greening of vegetation in northern China to a certain extent (Liu et al., 2012b). Moreover, changes in vegetation could affect the hydrologic cycle and, in particular, regulate the soil moisture content by adjusting the processes of ET and infiltration.

5.2. Relative contribution of afforestation practices

The hydrological effect of climate and vegetation changes largely depends on the scale of interest. Several studies concerning the Grain for Green Project on the Loess Plateau have shown that afforestation led to an increase in ET with a relatively small decline in soil moisture and runoff coefficients (Feng et al., 2016; Shao et al., 2019). These studies also stated that revegetation could aggravate the problem of sustainable water resource management, especially in the context of increased water use for anthropogenic activities. The in-situ observations further indicated that soil moisture in the afforestation area would reduce due to the conversion of agricultural land to forest (Jia et al., 2017a, 2017b). Zeng et al. (2018) indicated that more than 50% of the increase in ET was caused by the greening of vegetation at global scale.

Our simulation results also recognize the positive effects on ET and negative impacts on soil moisture content of afforestation in the arid and semi-arid regions. However, the relative impact of vegetation greening should depend on the magnitude of changes in vegetation greening, as well as the scale of the study area. In this study, ET showed an increasing trend under the combined effect of vegetation greening and precipitation increase in most part of TNR. While the soil moisture content in the Loess Plateau did not drop significantly due to the continuous increase in precipitation, especially, the significant increase since 2010. The soil moisture content even presented an upward trend in the northeastern and a small part of the northwestern TNR which experienced abundant precipitation. The effects of vegetation greenness were limited in contrast to changes caused by climatic factors for the entire TNR.

Moreover, the greening of vegetation was the result of a combination of climate change and afforestation (Liu and Gong, 2012; Wu et al., 2020). Further separating the impact of climate change on vegetation greening, the impact of afforestation on the hydrological cycle may be smaller. Xie et al. (2015) analyzed the influence of climate and vegetation on hydrological cycles and drew similar conclusions for this region. However, our study focused on a different time period and addressed some of the limitations that existed in Xie et al. (2015). The simulation uncertainties were expected to be reduced in this study due to the inclusion of dynamic LAI instead of static vegetation parameters and several meteorological stations. When the role of vegetation greening may be overestimated in previous studies, this study suggested that more attention should be paid to the hydrological effects of climate change in the TNR.

In this study, we also identified the effect of vapor pressure deficit (VPD) on ET dynamics. Changes in VPD gives a very small impact on the ET increase or decrease for the five basins in TNR; therefore, the results are not shown here. Increasing VPD may enhance ET to supplement atmospheric water demand. However, vegetation would respond to the VPD increase by closing stomata and thereby reducing ET (Massmann et al., 2019).

5.3. Uncertainties

Although some improvements have been made in this study, a few limitations exist, namely, factors relating to the control variable method employed in the attribution analysis. In this method, the impacts of the environmental factors on the hydrological cycle were estimated by simply removing the trend of either forcing variable. However, meteorological factors and vegetation are often interrelated in realistic scenarios (Ji, 1995; Zeng and Neelin, 2010). The offline assessment setting breaks the feedback of vegetation growth to regional water balance as the assumption that precipitation is a forcing variable. Li et al. (2018) found that increasing vegetation gives a positive feedback to precipitation in northern China and that declining vegetation would decrease precipitation in northeastern China during the period of 1982–2011. Neglecting these interactions may induce biased estimations of their hydrological effects.

Moreover, ET plays a crucial role in the water and energy balance (Hirano et al., 2017). The ET estimation algorithm formulated in the VIC model was based on the water balance process. However, the energy balance process should also be considered in the model simulation to achieve the most reliable ET estimation (Larsen et al., 2016; Liou and Kar, 2014). In this study, the energy balance process was not considered in the model simulation. Thus, the ET estimates may have substantial uncertainties.

In addition, other environmental factors also affect the hydrological cycle, such as precipitation intensity and model parameters. Zhou et al. (2011) indicated that the temporal pattern of precipitation may play a more important role in water yield and ET than the precipitation amount. Afforestation likely altered parameters of soil properties because of the accumulation of deciduous leaves on the surface and the growth of root system under the surface (Meng et al., 2016; Sauer et al., 2012; Shirato et al., 2004). And simply using dynamic vegetation parameters (i.e., LAI) cannot compensate for the uncertainties caused by changes in artificial land use types. Therefore, the VIC simulations with constant model parameters may hold biases, especially in the afforestation areas of this region. In addition, our study did not consider the impact of other human activities, such as agricultural irrigation, reservoir storage and check-dam construction, while these impacts on hydrological cycle are considerable at various spatial and temporal scale (Zhang et al., 2019).

6. Conclusions

In this study, the VIC model was employed to examine the influence of recent trends in climate change and vegetation greenness on the hydrological cycle in the TNR from 2000 to 2015. Despite the spatial heterogeneity, significant trends in precipitation were observed for over

39.9% (>5 mm/year) of the TNR, with a mean increase rate of 3.96 mm/year over the entire regions. The temperature fluctuation was minimal during the last 16 years. Under the contribution of afforestation programs, the vegetation LAI for the growing season exhibited a significant increase across the entire TNR. Therefore, the ET increased at a rate of 2.86 mm/year over the entire TNR during the study period. The spatial pattern of the ET was consistent with the changes in the LAI and precipitation. Regardless of an average increase of 1.72 mm/year over the entire region, the trends for soil moisture were variable across the different basins.

The results of the attribution analysis indicate that the evolutions of hydrological factors (ET, SM and runoff) are quite sensitive to vegetation greening only at relatively small scale where the magnitude of greening is high (e.g., some small catchments in the Loess Plateau), but they are still dominated by the change in precipitation at the regional scale. So the impact of vegetation greenness on the hydrological cycle is variable and depends on the magnitude of vegetation growth. This new finding implies that hydrological effect of vegetation greening may be overestimated at regional scale in the TNR by previous studies.

Afforestation might exacerbate environmental problems in the arid and semi-arid areas, such as reduced soil moisture content, especially in the areas with large magnitude of vegetation greening. To alleviate the environmental problems in the TNR, we propose paying attention to the impacts of climate change on the hydrological cycle in this region. The ecological afforestation programs need to be re-evaluated considering their negative effects on water conservation.

CRediT authorship contribution statement

Shanshan Meng: Conceptualization, Methodology, Software, Writing - original draft. **Xianhong Xie:** Conceptualization, Writing - review & editing, Funding acquisition. **Bowen Zhu:** Validation. **Yibing Wang:** Validation.

Declaration of Competing Interest

The authors declare that they have no known competing financial interests or personal relationships that could have appeared to influence the work reported in this paper.

Acknowledgments

This study was supported by grants from the National Key Research and Development Program of China (No. 2016YFA0600103, 2016YFC0401404) and the National Natural Science Foundation of China (No. 41971030).

Appendix A. Supplementary data

Supplementary data to this article can be found online at https://doi.org/10.1016/j.jhydrol.2020.125689.

References

An, R., et al., 2016. Validation of the ESA CCI soil moisture product in China. Int. J. Appl. Earth Observ. Geoinform. 48, 28–36. https://doi.org/10.1016/j.jag.2015.09.009.
Andréassian, V., 2004. Waters and forests: from historical controversy to scientific debate. J. Hydrol. 291 (1), 1–27. https://doi.org/10.1016/j.jhydrol.2003.12.015.
Bao, Z., et al., 2012. Attribution for decreasing streamflow of the Haihe River basin, northern China: climate variability or human activities? J. Hydrol. 460–461, 117–129. https://doi.org/10.1016/j.jhydrol.2012.06.054.
Bi, C., Bi, H., Sun, G., Chang, Y., Gao, L., 2014. Scale effects and variability of forest–water yield relationships on the Loess Plateau, China. Forestry Chronicle 90 (02), 184–191. https://doi.org/10.5558/tfc2014-036.
Bohn, T.J., Vivoni, E.R., 2015. Process-based characterization of evapotranspiration sources over the North American monsoon region. Water Resour. Res. 52 (1), n/a-n/a. https://doi.org/10.1002/2015WR017934.
Bonan, G.B., 2008. Forests and climate change: forcings, feedbacks, and the climate benefits of forests. Science 320 (5882), 1444–1449. https://doi.org/10.1126/science.1155121.
Bruijnzeel, L.A., 2004. Hydrological functions of tropical forests: not seeing the soil for the trees? Agric. Ecosyst. Environ. 104 (1), 185–228. https://doi.org/10.1016/j.agee.2004.01.015.
Buendia, C., Batalla, R.J., Sabater, S., Palau, A., Marcé, R., 2016. runoff trends driven by climate and afforestation in a Pyrenean Basin. Land Degrad. Develop 27 (3), 823–838. https://doi.org/10.1002/ldr.2384.
Cao, S., et al., 2011. Excessive reliance on afforestation in China's arid and semi-arid regions: Lessons in ecological restoration. Earth Sci. Rev. 104 (4), 240–245. https://doi.org/10.1016/j.earscirev.2010.11.002.
Chakravorty, A., Chahar, B.R., Sharma, O.P., Dhanya, C.T., 2016. A regional scale performance evaluation of SMOS and ESA-CCI soil moisture products over India with simulated soil moisture from MERRA-Land. Remote Sens. Environ. 186, 514–527. https://doi.org/10.1016/j.rse.2016.09.011.
Chen, C., et al., 2019. China and India lead in greening of the world through land-use management. Nat. Sustainability 2 (2), 122–129. https://doi.org/10.1038/s41893-019-0220-7.
Deng, H., et al., 2014. Dynamics of temperature and precipitation extremes and their spatial variation in the arid region of northwest China. Atmos. Res. 138, 346–355. https://doi.org/10.1016/j.atmosres.2013.12.001.
Dorigo, W., et al., 2017. ESA CCI Soil Moisture for improved Earth system understanding: State-of-the art and future directions. Remote Sens. Environ. 203, 185–215. https://doi.org/10.1016/j.rse.2017.07.001.
Duan, H., et al., 2011. Assessing vegetation dynamics in the Three-North Shelter Forest region of China using AVHRR NDVI data. Environ. Earth Sci. 64 (4), 1011–1020. https://doi.org/10.1007/s12665-011-0919-x.
Fang, H., Liang, S., Kuusk, A., 2003. Retrieving leaf area index using a genetic algorithm with a canopy radiative transfer model. Remote Sens. Environ. 85 (3), 257–270. https://doi.org/10.1016/S0034-4257(03)00005-1.
Feng, X., Fu, B., Lu, N., Zeng, Y., Wu, B., 2013. How ecological restoration alters ecosystem services: an analysis of carbon sequestration in China's Loess Plateau. Sci. Rep. 3, 2846.
Feng, X., et al., 2016. Revegetation in China's Loess Plateau is approaching sustainable water resource limits Nature. Clim. Change 6, 1019–1022. https://doi.org/10.1038/nclimate3092.
Gao, G., Fu, B., Wang, S., Liang, W., Jiang, X., 2016. Determining the hydrological responses to climate variability and land use/cover change in the Loess Plateau with the Budyko framework. Sci. Total Environ. 557–558, 331–342. https://doi.org/10.1016/j.scitotenv.2016.03.019.
Gerten, D., Schaphoff, S., Haberlandt, U., Lucht, W., Sitch, S., 2004. Terrestrial vegetation and water balance—hydrological evaluation of a dynamic global vegetation model. J. Hydrol. 286 (1), 249–270. https://doi.org/10.1016/j.jhydrol.2003.09.029.
Gocic, M., Trajkovic, S., 2013. Analysis of changes in meteorological variables using Mann-Kendall and Sen's slope estimator statistical tests in Serbia. Global Planet. Change 100 (Supplement C), 172–182. https://doi.org/10.1016/j.gloplacha.2012.10.014.
González-Zamora, Á., Sánchez, N., Pablos, M., Martínez-Fernández, J., 2018. CCI soil moisture assessment with SMOS soil moisture and in situ data under different environmental conditions and spatial scales in Spain. Remote Sens. Environ. https://doi.org/10.1016/j.rse.2018.02.010.
Gruber, A., Dorigo, W.A., Crow, W., Wagner, W., 2017. Triple collocation-based merging of satellite soil moisture retrievals. IEEE Trans. Geosci. Remote Sens. 55 (12), 6780–6792. https://doi.org/10.1109/TGRS.2017.2734070.
Guli, J., Liang, S., Yi, Q., Liu, J., 2015. Vegetation dynamics and responses to recent climate change in Xinjiang using leaf area index as an indicator. Ecol. Ind. 58 (Supplement C), 64–76. https://doi.org/10.1016/j.ecolind.2015.05.036.
Hamed, K.H., 2008. Trend detection in hydrologic data: the Mann-Kendall trend test under the scaling hypothesis. J. Hydrol. 349 (3), 350–363. https://doi.org/10.1016/j.jhydrol.2007.11.009.
Herron, N., Davis, R., Jones, R., 2002. The effects of large-scale afforestation and climate change on water allocation in the Macquarie River catchment, NSW, Australia. J. Environ. Manage. 65 (4), 369–381. https://doi.org/10.1006/jema.2002.0562.
Hirano, T., Suzuki, K., Hirata, R., 2017. Energy balance and evapotranspiration changes in a larch forest caused by severe disturbance during an early secondary succession. Agric. For. Meteorol. 232, 457–468. https://doi.org/10.1016/j.agrformet.2016.10.003.
Ji, J., 1995. A climate-vegetation interaction model: simulating physical and biological processes at the surface. J. Biogeogr. 22 (2/3), 445–451. https://doi.org/10.2307/2845941.
Jia, X., Shao, M.a., Zhu, Y., Luo, Y., 2017a. Soil moisture decline due to afforestation across the Loess Plateau, China. Journal of Hydrology, 546: 113-122. DOI:https://doi.org/10.1016/j.jhydrol.2017.01.011.
Jia, X., Wang, Y., Shao, M.A., Luo, Y., Zhang, C., 2017. Estimating regional losses of soil water due to the conversion of agricultural land to forest in China's Loess Plateau. Ecohydrology 10 (6), e1851. https://doi.org/10.1002/eco.1851.
Jia, Z., Liu, S., Xu, Z., Chen, Y., Zhu, M., 2012. Validation of remotely sensed evapotranspiration over the Hai River Basin, China. J. Geophys. Res.: Atmos. 117 (D13) https://doi.org/10.1029/2011JD017037.
Jung, M., et al., 2010. Recent decline in the global land evapotranspiration trend due to limited moisture supply. Nature 467 (7318), 951–954. https://doi.org/10.1038/nature09396.
Karthikeyan, L., Pan, M., Wanders, N., Kumar, D.N., Wood, E.F., 2017a. Four decades of microwave satellite soil moisture observations: Part 1. A review of retrieval

algorithms. Adv. Water Resour. 109, 106–120. https://doi.org/10.1016/j.advwatres.2017.09.006.
Karthikeyan, L., Pan, M., Wanders, N., Kumar, D.N., Wood, E.F., 2017b. Four decades of microwave satellite soil moisture observations: Part 2. Product validation and inter-satellite comparisons. Adv. Water Resour. 109, 236–252. https://doi.org/10.1016/j.advwatres.2017.09.010.
Larsen, M.A.D., et al., 2016. Calibration of a distributed hydrology and land surface model using energy flux measurements. Agric. For. Meteorol. 217, 74–88. https://doi.org/10.1016/j.agrformet.2015.11.012.
Li, G., Zhang, F., Jing, Y., Liu, Y., Sun, G., 2017. Response of evapotranspiration to changes in land use and land cover and climate in China during 2001–2013. Sci. Total Environ. 596–597 (Supplement C), 256–265. https://doi.org/10.1016/j.scitotenv.2017.04.080.
Li, Y., et al., 2018. Divergent hydrological response to large-scale afforestation and vegetation greening in China. Sci. Adv. 4 (5), eaar4182. https://doi.org/10.1126/sciadv.aar4182.
Liang, X., Lettenmaier, D.P., Wood, E.F., Burges, S.J., 1994. A simple hydrologically based model of land surface water and energy fluxes for general circulation models. Journal of Geophysical Research: Atmospheres (1984–2012), 99(D7): 14415-14428. DOI:https://doi.org/10.1029/94JD00483.
Liang, X., Wood, E.F., Lettenmaier, D.P., 1996. Surface soil moisture parameterization of the VIC-2L model: evaluation and modification. Global Planet. Change 13 (1), 195–206. https://doi.org/10.1016/0921-8181(95)00046-1.
Liou, Y.-A., Kar, S., 2014. Evapotranspiration estimation with remote sensing and various surface energy balance algorithms—a review. Energies 7 (5), 2821. https://doi.org/10.3390/en7052821.
Liu, J., et al., 2014. Spatiotemporal characteristics, patterns, and causes of land-use changes in China since the late 1980s. J. Geog. Sci. 24 (2), 195–210. https://doi.org/10.1007/s11442-014-1082-6.
Liu, J., Li, S., Ouyang, Z., Tam, C., Chen, X., 2008. Ecological and socioeconomic effects of China's policies for ecosystem services. Proc. Natl. Acad. Sci. 105 (28), 9477–9482. https://doi.org/10.1073/pnas.0706436105.
Liu, J., Zhang, Q., Hu, Y., 2012a. Regional differences of China's urban expansion from late 20th to early 21st century based on remote sensing information. Chin. Geogr. Sci. 22 (1), 1–14. https://doi.org/10.1007/s11769-012-0510-8.
Liu, J., et al., 2010. Spatial patterns and driving forces of land use change in China during the early 21st century. J. Geog. Sci. 20 (4), 483–494. https://doi.org/10.1007/s11442-010-0483-4.
Liu, L., et al., 2013. Mapping afforestation and deforestation from 1974 to 2012 using Landsat time-series stacks in Yulin District, a key region of the Three-North Shelter region, China. Environ. Monit. Assess. 185 (12), 9949–9965. https://doi.org/10.1007/s10661-013-3304-2.
Liu, R., Zhao, H., Zhao, X., Drake, S., 2011. Facilitative effects of shrubs in shifting sand on soil macro-faunal community in Horqin Sand Land of Inner Mongolia, Northern China. Eur. J. Soil Biol. 47 (5), 316–321. https://doi.org/10.1016/j.ejsobi.2011.07.006.
Liu, S., Gong, P., 2012. Change of surface cover greenness in China between 2000 and 2010. Chin. Sci. Bull. 57 (22), 2835–2845. https://doi.org/10.1007/s11434-012-5267-z.
Liu, Y., et al., 2012b. Spatial and temporal variations of forest LAI in China during 2000–2010. Chin. Sci. Bull. 57 (22), 2846–2856. https://doi.org/10.1007/s11434-012-5064-8.
Liu, Y., et al., 2016. Recent trends in vegetation greenness in China significantly altered annual evapotranspiration and water yield. Environ. Res. Lett. 11 (9), 094010 https://doi.org/10.1088/1748-9326/11/9/094010.
Ma, R., et al., 2017. Assimilation of remotely-sensed leaf area index into a dynamic vegetation model for gross primary productivity estimation. Rem. Sens. 9 (3), 188. https://doi.org/10.3390/rs9030188.
Ma, Z., Kang, S., Zhang, L., Tong, L., Su, X., 2008. Analysis of impacts of climate variability and human activity on streamflow for a river basin in arid region of northwest China. J. Hydrol. 352 (3), 239–249. https://doi.org/10.1016/j.jhydrol.2007.12.022.
Martens, B., et al., 2017. GLEAM v3: Satellite-based land evaporation and root-zone soil moisture. Geosci. Model Dev. 10 (5), 1903–1925. https://doi.org/10.5194/gmd-10-1903-2017.
Massmann, A., Gentine, P., Lin, C., 2019. When does vapor pressure deficit drive or reduce evapotranspiration? J. Adv. Model. Earth Syst. 11 (10), 3305–3320. https://doi.org/10.1029/2019MS001790.
Meng, S., Xie, X., Yu, X., 2016. Tracing temporal changes of model parameters in rainfall-runoff modeling via a real-time data assimilation. Water 8 (1), 19. https://doi.org/10.3390/w8010019.
Miralles, D., et al., 2011. Global land-surface evaporation estimated from satellite-based observations. Hydrol. Earth Syst. Sci. 15, 453–469. https://doi.org/10.5194/hess-15-453-2011.
Moore, R., Wondzell, S.M., 2005. Physical hydrology and the effects of forest harvesting in the Pacific Northwest: a review. JAWRA J. Am. Water Resour. Assoc. 41 (4), 763–784. https://doi.org/10.1111/j.1752-1688.2005.tb03770.x.
Nijssen, B., Schnur, R., Lettenmaier, D.P., 2001. Global retrospective estimation of soil moisture using the variable infiltration capacity land surface model, 1980–93. J. Clim. 14 (8), 1790–1808. https://doi.org/10.1175/1520-0442(2001)014<1790:GREOSM>2.0.CO;2.
Ning, J., Liu, J., Zhao, G., 2015. Spatio-temporal characteristics of disturbance of land use change on major ecosystem function zones in China. Chin. Geogr. Sci. 25 (5), 523–536. https://doi.org/10.1007/s11769-015-0776-8.
Peel, M.C., Mcmahon, T.A., Finlayson, B.L., 2010. Vegetation impact on mean annual evapotranspiration at a global catchment scale. Water Resour. Res. 46 (9), 2095–2170. https://doi.org/10.1029/2009WR008233.
Peng, J., Niesel, J., Loew, A., Zhang, S., Wang, J., 2015. Evaluation of satellite and reanalysis soil moisture products over southwest china using ground-based measurements. Rem. Sens. 7 (11), 15729. https://doi.org/10.3390/rs71115729.
Piao, S., et al., 2015. Detection and attribution of vegetation greening trend in China over the last 30 years. Glob. Change Biol. 21 (4), 1601–1609. https://doi.org/10.1111/gcb.12795.
Qin, Y., Yang, D., Lei, H., Xu, K., Xu, X., 2015. Comparative analysis of drought based on precipitation and soil moisture indices in Haihe basin of North China during the period of 1960–2010. J. Hydrol. 526, 55–67. https://doi.org/10.1016/j.jhydrol.2014.09.068.
Rodriguez-Iturbe, I., D'Odorico, P., Laio, F., Ridolfi, L., Tamea, S., 2007. Challenges in humid land ecohydrology: Interactions of water table and unsaturated zone with climate, soil, and vegetation. Water Resour. Res. 43 (9) https://doi.org/10.1029/2007WR006073.
Sauer, T.J., James, D.E., Cambardella, C.A., Hernandez-Ramirez, G., 2012. Soil properties following reforestation or afforestation of marginal cropland. Plant Soil 360 (1–2), 375–390. https://doi.org/10.1007/s11104-012-1258-8.
Shao, R., et al., 2019. Estimating the increase in regional evaporative water consumption as a result of vegetation restoration over the Loess Plateau, China. J. Geophys. Res.: Atmos. 124 (22), 11783–11802. https://doi.org/10.1029/2019jd031295.
Shen, X., An, R., Quaye-Ballard, J.A., Zhang, L., Wang, Z., 2016. Evaluation of the European space agency climate change initiative soil moisture product over china using variance reduction factor. JAWRA J. Am. Water Resour. Assoc. 52 (6), 1524–1535. https://doi.org/10.1111/1752-1688.12478.
Shirato, Y., Taniyama, I., Zhang, T.-H., 2004. Changes in soil properties after afforestation in Horqin Sandy Land, North China. Soil Sci. Plant Nutr. 50 (4), 537–543. https://doi.org/10.1080/00380768.2004.10408510.
Vose, J.M., et al., 2011. Forest ecohydrological research in the 21st century: what are the critical needs? Ecohydrology 4 (2), 146–158. https://doi.org/10.1002/eco.193.
Wang, G., et al., 2012. Assessing water resources in China using PRECIS projections and a VIC model. Hydrol. Earth Syst. Sci. 16 (1), 231–240. https://doi.org/10.5194/hess-16-231-2012.
Wang, S., et al., 2015. Reduced sediment transport in the Yellow River due to anthropogenic changes. Nat. Geosci. 9, 38. https://doi.org/10.1038/ngeo2602.
Wang, Y., Xie, X., Liang, S., Zhu, B., Yao, Y., Meng, S., Lu, C., 2020. Quantifying the response of potential flooding risk to urban growth in Beijing. Science of the Total Environment 705, 135868. https://doi.org/10.1016/j.scitotenv.2019.135868.
Wang, X.M., Zhang, C.X., Hasi, E., Dong, Z.B., 2010. Has the Three Norths Forest Shelterbelt Program solved the desertification and dust storm problems in arid and semiarid China? J. Arid Environ. 74 (1), 13–22. https://doi.org/10.1016/j.jaridenv.2009.08.001.
Wang, Z., et al., 2017. Spatiotemporal variability of reference evapotranspiration and contributing climatic factors in China during 1961–2013. J. Hydrol. 544 (Supplement C), 97–108. https://doi.org/10.1016/j.jhydrol.2016.11.021.
Wei, X., Zhou, X., Wang, C., 2003. The influence of mountain temperate forests on the hydrology in northeast China. Forest. Chronicle 79 (2), 297–300. https://doi.org/10.5558/tfc79297-2.
Wu, D., Xie, X., Tong, J., Meng, S., Wang, Y., 2020. Sensitivity of vegetation growth to precipitation in a typical afforestation area in the loess plateau: plant-water coupled modelling. Ecol. Model. 430, 109128 https://doi.org/10.1016/j.ecolmodel.2020.109128.
Xiao, Z., Liang, S., Sun, R., Wang, J., Jiang, B., 2015. Estimating the fraction of absorbed photosynthetically active radiation from the MODIS data based GLASS leaf area index product. Remote Sens. Environ. 171 (Supplement C), 105–117. https://doi.org/10.1016/j.rse.2015.10.016.
Xiao, Z., et al., 2014. Use of general regression neural networks for generating the GLASS leaf area index product from time-series MODIS surface reflectance. IEEE Trans. Geosci. Remote Sens. 52 (1), 209–223. https://doi.org/10.1109/TGRS.2013.2237780.
Xiao, Z., et al., 2016. Long-time-series global land surface satellite leaf area index product derived from MODIS and AVHRR surface reflectance. IEEE Trans. Geosci. Remote Sens. 54 (9), 5301–5318. https://doi.org/10.1109/TGRS.2016.2560522.
Xie, X., et al., 2015. Detection and attribution of changes in hydrological cycle over the Three-North region of China: climate change versus afforestation effect. Agric. For. Meteorol. 203, 74–87. https://doi.org/10.1016/j.agrformet.2015.01.003.
Xu, J., Yin, R., Li, Z., Liu, C., 2006. China's ecological rehabilitation: unprecedented efforts, dramatic impacts, and requisite policies. Ecol. Econ. 57 (4), 595–607. https://doi.org/10.1016/j.ecolecon.2005.05.008.
Yang, X., Yong, B., Ren, L., Zhang, Y., Long, D., 2017. Multi-scale validation of GLEAM evapotranspiration products over China via ChinaFLUX ET measurements. Int. J. Remote Sens. 38 (20), 5688–5709. https://doi.org/10.1080/01431161.2017.1346400.
Yang, X., Yong, B., Yin, Y., Zhang, Y., 2018. Spatio-temporal changes in evapotranspiration over China using GLEAM_V3.0a products (1980–2014). Hydrol. Res. 49 (5), 1330–1348. https://doi.org/10.2166/nh.2018.173.
Yao, Y., et al., 2019. Extended dependence of the hydrological regime on the land cover change in the three-north region of china: an evaluation under future climate conditions. Remote Sensing 11 (1). https://doi.org/10.3390/rs11010081.
Zeng, N., Neelin, J.D., 2010. The role of vegetation-climate interaction and interannual variability in shaping the African Savanna. J. Clim. 13 (15), 2665–2670. https://doi.org/10.1175/1520-0442(2000)013<2665:TROVCI>2.0.CO;2.

Zeng, Z., Peng, L., Piao, S., 2018. Response of terrestrial evapotranspiration to Earth's greening. Curr. Opin. Environ. Sustain. 33, 9–25. https://doi.org/10.1016/j.cosust.2018.03.001.

Zhang, J.C., Deangelis, D.L., Zhuang, J.Y., 2011. Effect of Afforestation on Soil and Water Conservation. Springer, New York.

Zhang, K., et al., 2015a. Influence of climate change on reference evapotranspiration and aridity index and their temporal-spatial variations in the Yellow River Basin, China, from 1961 to 2012. Quat. Int. 380–381, 75–82. https://doi.org/10.1016/j.quaint.2014.12.037.

Zhang, K., Xie, X., Zhu, B., Meng, S., Yao, Y., 2019. Unexpected groundwater recovery with decreasing agricultural irrigation in the Yellow River Basin. Agric. Water Manage. 213, 858–867. https://doi.org/10.1016/j.agwat.2018.12.009.

Zhang, L., Nan, Z., Yu, W., Ge, Y., 2015b. Modeling land-use and land-cover change and hydrological responses under consistent climate change scenarios in the Heihe River Basin, China. Water Resour. Manage. 29 (13), 4701–4717. https://doi.org/10.1007/s11269-015-1085-9.

Zhang, M., et al., 2017a. A global review on hydrological responses to forest change across multiple spatial scales: importance of scale, climate, forest type and hydrological regime. J. Hydrol. 546, 44–59. https://doi.org/10.1016/j.jhydrol.2016.12.040.

Zhang, W., Hu, G., Dang, Y., Weindorf, D.C., Sheng, J., 2016a. Afforestation and the impacts on soil and water conservation at decadal and regional scales in Northwest China. J. Arid Environ. 130, 98–104. https://doi.org/10.1016/j.jaridenv.2016.03.003.

Zhang, Y., et al., 2016b. Multiple afforestation programs accelerate the greenness in the 'Three North' region of China from 1982 to 2013. Ecol. Ind. 61, 404–412. https://doi.org/10.1016/j.ecolind.2015.09.041.

Zhang, Y., Yao, Y., Wang, X., Liu, Y., Piao, S., 2017b. Mapping spatial distribution of forest age in China. Earth Space Sci. 4 (3), 108–116. https://doi.org/10.1002/2016ea000177.

Zhao, H.-L., et al., 2007. Shrub facilitation of desert land restoration in the Horqin Sand Land of Inner Mongolia. Ecol. Eng. 31 (1), 1–8. https://doi.org/10.1016/j.ecoleng.2007.04.010.

Zhou, G., et al., 2011. Quantifying the hydrological responses to climate change in an intact forested small watershed in Southern China. Glob. Change Biol. 17 (12), 3736–3746. https://doi.org/10.1111/j.1365-2486.2011.02499.x.

Zhu, B., Xie, X., Meng, S., Lu, C., Yao, Y., 2020. Sensitivity of soil moisture to precipitation and temperature over China: present state and future projection. Sci. Total Environ. 705, 135774 https://doi.org/10.1016/j.scitotenv.2019.135774.

Zhu, J.J., et al., 2017. Assessment of the world largest afforestation program: success, failure, and future directions. bioRxiv, 105619. https://doi.org/10.1101/105619.

Zhu, Z., et al., 2016. Greening of the Earth and its drivers. Nat. Clim. Change 6 (8), 791–795. https://doi.org/10.1038/nclimate3004.